Porous architecture and thermal properties of thermal barrier coatings deposited by suspension plasma spray

Yongli Zhao, Juhong Wen, François Peyraut, Marie-Pierre Planche, Shantanu Misra, Bertrand Lenoir, Jan Ilavsky, Hanlin Liao, Ghislain Montavon

Porous architecture and thermal properties of thermal barrier coatings deposited by suspension plasma spray

Yongli Zhao [ab*], Juhong Wen [a], François Peyraut [b], Marie-Pierre Planche [b], Shantanu Misra [c] Bertrand Lenoir [c], Jan Ilavsky [d], Hanlin Liao [b], Ghislain Montavon [b]

[a] School of Mechanical and Automotive Engineering, Shanghai University of Engineering Science, 201620, China

[b] ICB UMR 6303, CNRS, Université de Bourgogne Franche-Comté, UTBM, 90010 Belfort, France

[c] Institut Jean Lamour, UMR 7198 CNRS, Université de Lorraine, 2 allée André Guinier-Campus ARTEM, BP 50840, 54011 Nancy, France

[d] Advanced Photon Source, Argonne National Laboratory, 9700 S. Cass Avenue, Argonne, IL 60439, USA

*Corresponding author: E-mail: zyl@sues.edu.cn

Abstract:

Besides the intrinsic low heat transfer capability of material, the thermal insulation property of thermal barrier coatings (TBCs) also rely on their microstructures. For better understanding the relationship between process parameters, porous architecture, and thermal properties of coatings, YSZ coatings were firstly manufactured by suspension plasma spray (SPS). Afterwards their total porosities were characterized by using the technique of X-ray

transmission, the nano/submicro pores in those coatings were detected with Ultra-Small Angle X-ray Scattering (USAXS), and the thermal properties of coatings were measured using the laser flash method. The results indicated that: i) the porous architecture of SPS coatings can be tailored by adapting process parameters. ii) increasing total porosity is an effective means for reducing the heat transfer capability of SPS coatings. iii) nano/submicro pores have higher influence sensitivity on thermal properties than that of larger pores. Increasing the content of nano-submicro pores is therefore more effective for improving the thermal insulation property of SPS coatings. The potential of SPS technique for fabricating TBCs was discussed as well.

Keywords: thermal barrier coating; suspension plasma spray; YSZ coating; porous architecture; thermal property

1 Introduction

Thermal barrier coatings (TBCs) are being used in gas-turbine engines to protect metallic components from thermal damage and thereby improve the engine energy efficiency [1]. The most widely employed techniques for manufacturing TBCs are Electron Beam-Physical Vapor Deposition (EB-PVD) and Atmospheric Plasma Spraying (APS) [1]. For the technique of EB-PVD, a specific columnar structured TBCs with higher strain tolerance leading to higher lifetime can be achieved. However, the high investment costs and the low deposition rates limits its applications. In contrast to EB-PVD, versatility and low deposition costs make APS an

attractive technique for such industrial applications [2, 3].

Finely structured or nanostructured coatings have been proven exhibiting superior performances compared to the micrometer-sized coatings [3, 4], such as lower thermal conductivity and higher strain tolerance. However, the powders sprayed using APS technique are normally tens of microns leading to micrometer-sized features in coatings [5]. To form finely structured coatings by thermal spraying technique, a feasible solution consists in reducing the size of the precursors to a sub-micrometric or nanometric scale. But these smaller particles are very difficult to feed using conventional equipment since they have poor flowability and tend to form larger aggregates that can cause blocking in the injection path. Thanks to the use of liquid carrier, suspension plasma spray (SPS) enables to inject submicrometric or nanometric size powders into the hot flame and allows to manufacture finely structured coatings. In the last decade, SPS has continuously gained increasing interest in the scientific world and is considered as one of the most promising emerging process to form finely coatings [3, 6].

Ceramics with low thermal conductivity (e.g. zirconia and alumina) are generally chosen as TBC top coat material. The thermal resistance of TBCs depends not only on the thermophysical properties of the ceramics, but also on their microstructure. Porous architecture of coatings, such as the size, shape, orientation and volumetric percentage of pores, could significantly influence coating properties [7]. Therefore, it needs to be quantitatively characterized and carefully considered for improving the performance of TBCs.

The quantification of pores in coatings can be performed with numerous common techniques using imaging [8], physical [9, 10], and electrochemical [9] approaches. However, the limited SEM resolution makes the imaging approach difficult to take into consideration the pores smaller than 100 nm. In addition to the measurement resolution, another disadvantage for physical and electrochemical approaches is their incapable to detect the closed pores. Therefore, by using these methods, the detection of nano-submicro pores is challenging and the total porosity of coating is usually underestimated. To solve the challenges in characterization of the nano-submicro pores, Ekberg et al. [11] employed Nuclear magnetic resonance (NMR) cryoporometry to characterize SPS coatings and discriminated successfully the pore size at the range of 5 to 500 nm. Klement et al. [10] used x-ray microscopy (XRM) to reconstruct a 3D imaging of pores and cracks at a resolution down to 50 nm. In order to characterize the pores in SPS coatings within the whole range, Ultra-Small Angle X-ray Scattering (USAXS) and X-ray transmission technique were applied in the current study. USAXS was used to characterize the nano-submicro pores due to its unprecedented capability in measuring very small pore sizes [12]. However, USAXS is not suitable to measure pores over a few micrometer in size. In order to accurately measure the total porosity of coatings, X-ray transmission technique was employed because it is a non-destructive test without any limitation of resolution [13].

In this study, Yttria-stabilized Zirconia (YSZ) coatings were firstly manufactured by SPS technique with different process parameters. The porous architecture of the coatings were

then characterized by using X-ray transmission and Ultra-Small Angle X-ray Scattering. Afterward the effect of process parameters on coating porous architecture, the correlation of the porous architecture and the thermal properties, the influence sensitivity of pore size on the thermal properties were investigated and discussed in detail. The aim of this study is to get a better understanding of the porous architecture and thermal properties of SPS coatings.

2 Experimental procedure

2.1. Suspension preparation

The initial materials are three types of YSZ (8 wt.% yttria, 3 wt.% alumina, Saint-Gobain ZirPro Co., Ltd.) with different particle sizes (D50 = 100, 230, and 360 nm). Their morphologies analyzed by SEM are shown in Fig.1. These powders with different mass load (20 wt.% and 25 wt.%) were dispersed in ethanol to prepare suspensions. Prior to adding of the YSZ powder, Dolapix et85 (Zschimmer & Schwarz, Germany) was added into the liquid phase for reaching the optimum suspension dispersion. In order to break down any agglomerate present, the suspensions were stirred with a magnetic stirrer and dispersed with an ultrasonic probe (UP 400S, Dr Hielscher GmbH, Germany). A twin-fluid atomizer developed with the Saint-Gobain company was used to inject the suspension into the plasma jet [12]. The vital parameters of suspension atomization was optimized by employing the shadowgraph technique with the help of the equipment SprayCam (Control Vision Inc, USA) [14]. The suspension feed rate was equal to about 45 g/min in all experiments.

2.2 Coating deposition

The plasma torch used for coating deposition was the atmospheric plasma ProPlasma torch (Saint-Gobain Coating Solutions, Avignon, France). It equipped with a 6.5 mm diameter anode and worked on the “high performance” mode. The working gases were a mixture of 50 L/min Argon and 10 L/min Hydrogen and the applied electric power was constant and equal to 41 kW. The plasma torch was attached to a 6-axis robotic arm with a scan speed of 1000 mm/s. The twin-fluid atomizer was positioned 6 mm downstream the anode face, and 10 mm perpendicularly to the torch axis. The details of the sketch of the set-up can be viewed at our previous work [12]. Stainless steel (304L, thickness = 10 mm, diameter = 25 mm) was used as substrate. They were polished or grit-blasted to obtain different surface topologies and their surface roughness were measured using 3D profilometer (Altisurf 500, France). In order to reduce the interface defects in the coatings, all substrates were preheated to 300 ℃ with the plasma jet before coating deposition [6]. To minimize the effect of substrate temperature on coating formation, the deposition temperature was monitored using an infrared thermometer and kept in the range from 300 to about 600 ℃. During the spray process, compressed air with the flow rate 110 SLPM was used as cooling gas. As coatings need to be removed from the substrates for the measurement using USAXS and x-ray transmission, no metallic bond coat layer was used between substrates and as-prepared YSZ coatings. The main process parameters of fabrication are listed in Table 1.

2.3 Porous architecture characterizations

The microstructural observations of as-sprayed YSZ coatings were performed using field emission scanning electron microscopy (JSM-7800F, JEOL, Japan). The observed samples

were manually cracked and sputtered with a thin gold layer to allow the ceramic layers to be observed clearly. Two techniques, X-ray transmission and Ultra-Small-Angle X-ray Scattering, were employed to characterize the porous architecture of coatings. Both of them were carried out at 9ID-C USAXS/SAXS/WAXS instrument (Argonne National Laboratory, Argonne, IL, USA) [15]. The experiments were conducted by X-ray energy of 16.9 keV with a beam size of 0.8 x 0.8 mm^2. Prior to the measurements, the YSZ coatings were removed from substrates by acid pickling in Aqua Regia. The free-standing coatings were then cleaned with deionized water and ethanol and finally dried in environment.

X-ray transmission technique was used to measure the total porosity of YSZ coatings. Based on the known density and chemical composition, the linear absorption coefficient of X-rays through YSZ solid phase can be calculated using theoretical models [16], and equals to 73.39 cm^{-1}. The solid phase thickness through which the X-ray beam passes is then calculated using the linear absorption coefficient (Beer's law). Finally, the total porosity of SPS coatings can be calculated using the following equation:

$$P_t = 1 - \frac{SPT}{THK} \qquad \text{Eq.1}$$

where P_t represents the total porosity, *SPT* the solid phase thickness and *THK* the measured coating thickness.

Ultra-Small-Angle X-ray Scattering was employed to evaluate the nano/submicro pores in the YSZ coatings [12]. Data included in this study are combined USAXS and SAXS data, spanning extended range of scattering vectors, *q*, from 10^{-4} to 1 $Å^{-1}$ [9, 17] .

$$q = \frac{4\pi}{\lambda \ sin(\theta)} \quad \text{Eq.2}$$

where λ is the wavelength of the X rays and 2θ is the scattering angle. WAXS data are not included in the present research as they did not bring in any new information. Scattering data were reduced using data reduction programs Indra and Nika [15]. Data were placed on absolute intensity scale using standard instrument calibration methods. Size distribution of pores was analyzed using Irena package [18].

2.4. Thermal property measurements

The thermal diffusivity, α, of as-sprayed SPS coatings prepared in the form of discs (10 mm in diameter) were measured with the laser-flash technique on a LFA 427 (Netzsch, Germany) in the temperature range from 25 to 850 ℃. Prior to measurement, the samples were spray-coated with a thin layer of graphite to increase absorption and emission on the respective surfaces. The thermal diffusivity, determined using the improved Cape-Lehmann model [19], was then used to calculate the thermal conductivity λ via the formula:

$$\lambda = \alpha \times C_p \times \rho \quad \text{Eq.3}$$

where C_p is the specific heat capacity and ρ the density of coating. The specific heat capacity of the YSZ material was measured using a DSC 404C differential scanning calorimeter (Netzsch, Germany). The density of coating was calculated via the following expression:

$$\rho = \rho_0 \times (1 - P_t) \quad \text{Eq.4}$$

where ρ_0 is the density of dense YSZ powder (5 mol% Y_2O_3 stabilized zirconia powder) which was estimated on 6.0 g/cm^3 and P_t is the total porosity of SPS coating.

3 Results

3.1 Porous architecture of coatings

Figure 2 presents a typical SEM fractography of as prepared YSZ coating. It can be seen that the coating exhibits a granular and porous structure. As the arrows indicate in Fig 2b, the coating is made of flattened lamellae (L), spherical particles (M), and irregular particles (U). The lamellae correspond to fully molten particles that spread upon impact. The spherical particles were from the fully molten particles that would solidify prior their impact. The irregular particles should be the particles that is not well molten and therefore exhibit the shape of the initial feedstock. The pores contained in the microstructure are formed in the gap between these particles and flattened lamellae. These pores are in a wide dimension range from nanometer up to several micrometers.

The results of measurement of X-ray transmission for the coatings are given in Table 2. The second column presents the actual thickness of coatings while the third shows the solid phase thickness calculated according to the X-ray transmission coefficient. The total porosities of coatings were then obtained by reporting the values of the second and third columns of Table 2 in Eq 1. The results are shown in the second column of Table 3.

USAXS were also carried out on the all SPS coatings. Due to USAXS technique is not suitable to detect the pores over a few micrometer in size, pores larger than 1 μm are ignored and not measured in this study. The detected pore size distributions of the as-prepared coatings are

showed in Fig 3. The contents of these nano-submicro pores in the coatings are calculated by integrating their size distributions over all sizes (third column of Table 3).

Table 3 summarizes the porous architecture of the as prepared SPS coatings. Since the pores smaller than 1 μm have been accurately characterized by using USAXS and the total porosity of coatings were measured with the technique x-ray transmission, the coarse portion of pores (P_b, pore size ≥ 1 μm) can be therefore calculated using the following equation:

$$P_b = P_t - P_s \qquad \text{Eq.5}$$

where P_t represents the total porosity, P_s the content of the pores smaller than 1 μm. The contents of the pores larger than 1 μm are listed in the last column of Table 3. It is noted that the coating porosity are tailored in a large range, the total porosity varying from about 28% to about 44%, and the nano-submicro pores content (pore size < 1 μm) from about 10% to 15%. The process parameters have therefore a significant influence on the total porosity and the pore size distribution of SPS coatings. Consequently, it should be possible to tailor the porous architecture of SPS coatings by controlling the spray conditions.

3.2 Thermal properties of coatings

Figure 4 presents the evolutions of thermal diffusivity as a function of temperature for SPS coatings manufactured using the process parameters sets presented in Table 1. It was found that the thermal diffusivities are in the range of 0.26 to 0.55 mm^2/s. The coating S1 has the highest thermal diffusivity, whereas the lowest thermal diffusivity is obtained for coating S5 and

S6.

Thermal conductivity of the coatings was calculated by Eq.3 and their evolution with temperature are shown in Fig.5. The values of thermal conductivity obtained for the temperature from 25 up to 850 ℃ are in the range between 0.5 and 1.1 $Wm^{-1}K^{-1}$ for the studied coatings. In this studied range, the coating S1 has the highest thermal conductivity and coating S6 the lowest, in accordance with the thermal diffusivity evolution.

4 Discussions

4.1 Effect of process parameters on coating porous architecture

It is observed in Fig 6 that 50% of the nano-submicro pores in the coatings are smaller than 65 nm. One other interesting insight is that 90% of the nano-submicro pores in all the coatings are smaller than 360 nm, which is the biggest size of initial powders used in this study. It is also remarked in Fig 6 that coating S2 has the smallest average nano-submicro pore size, followed by coating S3 and coating S4. Since the corresponding initial power size of these three coatings are 100, 230, and 360 nm respectively (Table 1), it seems that the smaller the initial powder size, the smaller the average nano-submicro pore size in coatings. The reason is most probably due to the formation of void during the deposition of coating. Some of the void spaces are formed by the compact stacking of quasi-spherical particles. Therefore, smaller particles will result in smaller void spaces. Nevertheless, this point needs to be more deeply investigated and questioned in further study.

4.2 Correlation of thermal properties with total porosity

Figure 7 shows both total porosity and thermal diffusivity of each coating. Since the thermal diffusivity is temperature dependent (Fig. 4), we have averaged it in the range from 25 to 850 ℃. It is noted that the coating's thermal diffusivity decreases if the coating porosity increases. Coating S1 gives for example the lowest porosity (28.2%) and the highest thermal diffusivity (0.41 mm^2/s), while coating S6 gives the highest porosity (43.9%) and the lowest thermal diffusivity (0.29 mm^2/s). A similar trend is observed for the thermal conductivity (Fig.8), with a decrease from 0.98 $Wm^{-1}K^{-1}$ (coating S1) to 0.55 $Wm^{-1}K^{-1}$ (coating S6). The higher thermal insulation property of coatings resulting from higher porosity can be explained by the following considerations:

i) During the coating formation, gases from the atmosphere are entrapped in the coating which results in porosity. These gases have a much lower thermal conductivity than the YSZ material [20], at room temperature and atmospheric pressure, the air conductivity is about 0.025 $Wm^{-1}K^{-1}$, dense YSZ is above 2.5 $Wm^{-1}K^{-1}$. Therefore, the higher the porosity in the coating, the lower its thermal conductivity.

ii) Pore boundaries produce scattering of the lattice waves (phonons) that transport the thermal energy through the coating [21-23]. Assuming that the average pore size is the same, coatings with higher porosity should have larger boundaries than that of coatings with lower porosity. Therefore, higher porosity level in the coating will effectively reduce the heat transfer.

4.3 Sensitivity analysis of thermal properties with respect to pore size

As discussed above, there is a direct correlation between the coating total porosity and the thermal properties. However, this correlation is not enough to fully understand the influence of coating porous architecture on the thermal properties. Actually, according to the results in section 3, coatings S1 and S2 have almost the same total porosity (28.2% and 28.1%, respectively – Table 3), but the thermal diffusivity and thermal conductivity of coating S2 is lower than that of coating S1 (Fig. 4 and 5). On another side, it is not possible to focus exclusively on the content of nano-submicro pores because coatings S4 and S5 have almost a similar content (12.3% and 12.2%, respectively), but a significant difference was observed between both regarding their thermal diffusivities and thermal conductivities (Fig. 4 and 5). That indicates that total porosity and pore size distribution must be accounted both. We have therefore introduced a linear model including the content of big pores P_b (%, pore size ≥ 1 µm), as well as the content of nano-submicro pores P_s (%, pore size < 1 µm):

$$T = c_0 + c_1 * P_b + c_2 * P_s \qquad \text{Eq.6}$$

where T is the thermal diffusivity (mm^2/s) or the thermal conductivity ($Wm^{-1}K^{-1}$), and c_0~c_2 represent the correlation coefficients. These coefficients were identified in order to match as well as possible the numerical results coming from Eq 6 with the experimental data.

The results of the identification process are presented in Table 4. The coefficients of determination R^2 indicating the efficiency of the identification process are equal to 0.998 and 0.997 for thermal diffusivity and thermal conductivity, respectively. These excellent scores,

very close to 1, prove the high ability of Eq 6 to fit properly the experiments. Another interesting insight concerns the coefficient c_2 which is much greater than c_1 for both thermal diffusivity and thermal conductivity, meaning that the impact of c_2 is much higher than c_1. In this condition, if we want to adjust the thermal insulation property of the coating in a given range by changing the value of one of the two independent variables P_s or P_b, the variation range of P_b will be larger than that of P_s. This indicates that the nano-submicro pores has a higher influence than that of big pores.

The high influence of nano-submicro pores on the coating thermal resistance can be attributed to the sharp drop in thermal conductivity of air trapped in small pores. Actually, when the pore size shifts from the micro- to nano-scale, the thermal conductivity of gas entrapped in the pore will be decreased due to the Knudsen effect [9, 24]. Consequently, the evolution of the thermal conductivity of air can be expressed as [9, 25, 26]:

$$\lambda_{air} = \lambda_{atm} \frac{1}{1+CT/(Pd)} \qquad \text{Eq.7}$$

where λ_{atm} is the gas conductivity at room temperature and atmospheric pressure (0.025 $Wm^{-1}K^{-1}$), d is the pore size, and the coefficient C is a constant for a given temperature and pressure. Figure 9 displays the evolution described by Eq 7 as a function of the pore size under the condition of T=25 ℃ and P =1 atm. It can be seen that the smaller the pore size, the lower the thermal conductivity of the gas entrapped and therefore the higher the thermal resistance provided by the pore. Furthermore, this tendency is more pronounced when the pore size is close to, or smaller, than the mean free path length of the air (about 60 nm for air at room temperature under atmospheric pressure). According to the expression of Eq 7, one

can see that the influence trend of pore size on the gas conductivity should be similar at different temperatures and different pressures, as λ_{atm} , coefficient C, T, and P are certain values for a given condition. For the SPS coatings in this study, more than 50% of the nano-submicro pores are smaller than 65 nm (see Fig 6). Therefore, these nanopores could play an important role in weakening heat transfer capability of the coating.

Furthermore, as discussed above, the scattering of the phonons in the pore boundary may also result in the high influence sensitivity of nano-submicro pores. At the same total porosity, coatings with more nano-submicro pores have more pore boundaries and thereby the heat transfer is significantly reduced.

4.4 Potential of SPS coatings as TBCs

Figure10 presents some typical values of thermal conductivity extracted from the literature [27-30], with YSZ coating prepared by techniques different than the one used in this paper. From the left to the right of Fig. 10, it is noted that:

i) Thermal conductivity of dense YSZ material is more than 2.5 $Wm^{-1}K^{-1}$ [27].

ii) Thermal conductivity of EB-PVD YSZ coatings was above 1.5 $Wm^{-1}K^{-1}$ [28].

iii) The YSZ coatings prepared by conventional APS technique is about 1.2 $Wm^{-1}K^{-1}$ for high density coatings and about 0.9 $Wm^{-1}K^{-1}$ for low density coatings [29, 30].

Compared to these coatings, the SPS coatings obtained in this study have a lower thermal conductivity (typically 0.5 - 0.9 $Wm^{-1}K^{-1}$). Therefore, from the point of view of the thermal insulation property, SPS technique is very promising for the fabrication of thermal barrier

coatings (TBCs). Nevertheless, it should be noted that, in addition to the low heat transfer capability, other coating performances in terms of thermal cycle fatigue (TCF), adhesion strength and erosion resistance need to be investigated and questioned in further studied for an industrial TBCs.

5 Conclusions

Suspension plasma sprayed YSZ coatings with different porous architecture were fabricated. Thermal properties of these coatings were characterized and analyzed. The main results are summarized as follows:

i) The porous architecture of SPS coatings has a direct correlation with process parameters. It should therefore be possible in further developments to tailor the porous architecture of SPS coatings by controlling the spray conditions.

ii) Coating total porosity has an important effect on the coating thermal properties. Increasing total porosity is an effective means for reducing the heat transfer capability of SPS coatings.

iii) Nano-submicro pores have higher influence on coating thermal properties than that of larger pores. Increasing the content of nano-submicro pores is therefore an effective way for improving the thermal insulation property of SPS coatings.

iv) Compared to other conventional techniques (APS, EB-PVD), SPS coatings have a lower thermal conductivity. Therefore, SPS technique is very promising for the fabrication of thermal barrier coatings.

Acknowledgments

This research used resources of the Advanced Photon Source, a U.S. Department of Energy (DOE) Office of Science User Facility operated for the DOE Office of Science by Argonne National Laboratory under Contract No. DE-AC02-06CH11357. This research was also sponsored by startup research foundation of Shanghai University of Engineering Science No. 201980.

References

[1] N.P. Padture, M. Gell, E.H. Jordan, Thermal barrier coatings for gas-turbine engine applications, Science, 296(5566) (2002), p.280-284

[2] D. Zhou, et al., *Sintering behavior of columnar thermal barrier coatings deposited by axial suspension plasma spraying (SPS).* Journal of the European Ceramic Society, **39**(2) (2019), p. 482-490

[3] A. Vardelle, et al., The 2016 Thermal Spray Roadmap. Journal of Thermal Spray Technology, 25(3) (2016), p. 1376-1440

[4] Y. Wang, et al., A novel structured suspension plasma sprayed YSZ-PTFE composite coating with tribological performance improvement. Surface and Coatings Technology, 358 (2019), p. 108-113

[5] P. Fauchais, et al., Engineering a new class of thermal spray nano-based microstructures from agglomerated nanostructured particles, suspensions and solutions: an invited review. Journal of Physics D: Applied Physics, 44(9) (2011), p.

093001

[6] Y. Zhao, et al., Influence of substrate properties on the formation of suspension plasma sprayed coatings, J. Therm. Spray Technol. 27 (1) (2018) 73-83

[7] F. Cernuschi, et al., Modelling of thermal conductivity of porous materials: application to thick thermal barrier coatings. Journal of the European Ceramic Society, 24(9) (2004), p. 2657-2667

[8] Y. Zhao, et al., Experiments, statistical analysis, and modeling to evaluate the porosity influence in SPS coatings, J. Therm. Spray Technol. 28 (2019) 76-86

[9] A. Bacciochini, et al., Quantification of void network architectures of suspension plasma-sprayed (SPS) yttria-stabilized zirconia (YSZ) coatings using Ultra-small-angle X-ray scattering (USAXS). Materials Science and Engineering: A, 528(1) (2010), p. 91-102.

[10] U. Klement, J. Ekberg, S.T. Kelly, 3D analysis of porosity in a ceramic coating using X-ray microscopy, J. Therm. Spray Technol. 26 (3) (2017) 456–463.

[11] J. Ekberg, L. Nordstierna, U. Klement, Porosity investigation of yttria-stabilized zirconia topcoats using NMR cryoporometry, Surf. Coat. Technol. 315 (2017) 468–474.

[12] Y. Zhao, et al., Evaluation of nano/submicro pores in suspension plasma sprayed YSZ coatings. Surface and Coatings Technology, (2019), https://doi.org/10.1016/j.surfcoat.2019.125001.

[13] Y. Zhao, et al., Parametric Analysis and Modeling for the Porosity Prediction in Suspension Plasma-Sprayed Coatings. Journal of Thermal Spray Technology, 29(1)

(2020), p. 51-59.

[14] E. Aubignat, et al., Optimization of the injection with a twin-fluid atomizer for suspension plasma spray process using three non-intrusive diagnostic tools. Journal of Visualization, 19(1) (2016), p. 21-36.

[15] J. Ilavsky, et al., Development of combined microstructure and structure characterization facility for in situ and operando studies at the Advanced Photon Source. Journal of Applied Crystallography, 51(3) (2018), p. 867-882.

[16] D.T. Cromer, D.A. Liberman, Anomalous dispersion calculations near to and on the long-wavelength side of an absorption edge. Acta Cryst, A37 (1981), p. 267-268.

[17] K. Kishitake, H. Era, F. Otsubo, Characterization of plasma sprayed Fe-17Cr-38Mo-4C amorphous coatings crystallizing at extremely high temperature. Journal of Thermal Spray Technology, 5(3) (1996), p. 283-288.

[18] J. Ilavsky, P.R. Jemian, Irena: tool suite for modeling and analysis of small-angle scattering. Journal of Applied Crystallography,. 42(2) (2009), p. 347-353.

[19] J. Blumm, J. Opfermann, Improvement of the mathematical modeling of flash measurements. High Temperatures. High Pressures,. 34(5) (2002), p. 515-521.

[20] K.W. Schlichting, N.P. Padture, P.G. Klemens, Thermal conductivity of dense and porous yttria-stabilized zirconia. Journal of Materials Science, 36(12) (2001), p. 3003-3010.

[21] J.R. Nicholls, Methods to reduce the thermal conductivity of EB-PVD TBCs. Surface and Coatings Technology, 151 (2002), p. 383-391.

[22] P.K. Schelling, S.R. Phillpot, Mechanism of Thermal Transport in Zirconia and Yttria -

Stabilized Zirconia by Molecular‐Dynamics Simulation. Journal of the American Ceramic Society, 84(12) (2001), p. 2997-3007.

[23] P. Klemens, Theory of thermal conduction in thin ceramic films. International journal of thermophysics,. 22(1) (2001), p. 265-275.

[24] J.H. Qiao, et al., Knudsen Effect on the Estimation of the Effective Thermal Conductivity of Thermal Barrier Coatings. Journal of Thermal Spray Technology, 22(2) (2013), p. 175-182.

[25] I.O. Golosnoy, A. Cipitria, T.W. Clyne, Heat Transfer Through Plasma-Sprayed Thermal Barrier Coatings in Gas Turbines: A Review of Recent Work. Journal of Thermal Spray Technology, 18(5) (2009), p. 809-821.

[26] E. Litovsky, M. Shapiro, A. Shavit, Gas pressure and temperature dependences of thermal conductivity of porous ceramic materials: Part 2, refractories and ceramics with porosity exceeding 30%. Journal of the American Ceramic Society, 79(5) (1996), p. 1366-1376.

[27] D.R. Clarke, S.R. Phillpot, Thermal barrier coating materials. Materials Today, 8(6) (2005), p. 22-29.

[28] A. Feuerstein, et al., Technical and Economical Aspects of Current Thermal Barrier Coating Systems for Gas Turbine Engines by Thermal Spray and EBPVD: A Review. Journal of Thermal Spray Technology, 17(2) (2008), p. 199-213.

[29] Raghavan, S., et al., The effect of grain size, porosity and yttria content on the thermal conductivity of nanocrystalline zirconia. Scripta Materialia, 39(8) (1998).: p. 1119-1125.

[30] N. Curry, et al., Influence of bond coat surface roughness on the structure of axial

suspension plasma spray thermal barrier coatings — Thermal and lifetime performance. Surface and Coatings Technology, 268 (2015), p.15-23.

Figure Captions

Fig.1 SEM images of the morphology of YSZ powders: (a) 100 nm, (b) 230 nm, and (c) 360 nm

Fig.2 Fractography images of as prepared SPS coating (a) overview showing (b) Image at higher magnification

Fig.3 Size distribution of nano-submicro pores in SPS coatings

Fig.4 Thermal diffusivity of SPS coatings as a function of temperature

Fig.5 Thermal conductivity of SPS coatings as a function of temperature

Fig.6 Cumulative percentages of nano-submicro pores in SPS coatings

Fig.7 Thermal diffusivity of SPS coatings and their corresponding total porosities

Fig.8 Thermal conductivity of SPS coatings and their corresponding total porosities

Fig.9 Thermal conductivity evolution of air trapped in nano-submicro pores (Eq.7)

Fig.10 Comparison of thermal conductivity for YSZ coatings prepared by different techniques

Tables

Table1 Process parameters of the experimental runs to prepare coatings

Sample No.	Suspension mass load (wt.%)	Powder size (μm)	Spray distance (mm)	Spray step (mm)	Substrate roughness (μm)
S1	25	0.36	40	6	0.16
S2	20	0.1	40	6	2.45
S3	25	0.23	40	6	2.45
S4	20	0.36	40	3	3.51
S5	20	0.36	50	3	3.51
S6	25	0.36	50	12	3.51

Table 2 Results of coating porosity measured by X-Ray transmission

Sample No.	Coating thickness (μm)	Solid phase thickness (μm)
S1	338	242
S2	228	164
S3	235	166
S4	251	164
S5	180	103
S6	230	129

Table 3 Summary of the porous architecture in SPS coatings

Sample No.	Total porosity (%)	Content of nano-submicro pores (pore size < 1 μm) (%)	Content of big pores (pore size ≥ 1 μm) (%)
S1	28.2	10.1	18.1
S2	28.1	15.0	13.1
S3	29.3	14.2	15.0
S4	34.7	12.3	22.4
S5	42.6	12.2	30.4
S6	43.9	11.7	32.2

Table.4 Identified coefficients of Eq 6

	c_0	c_1	c_2	R^2
T=thermal diffusivity	0.653	0.007	0.012	0.998
T=thermal conductivity	1.844	0.026	0.039	0.997

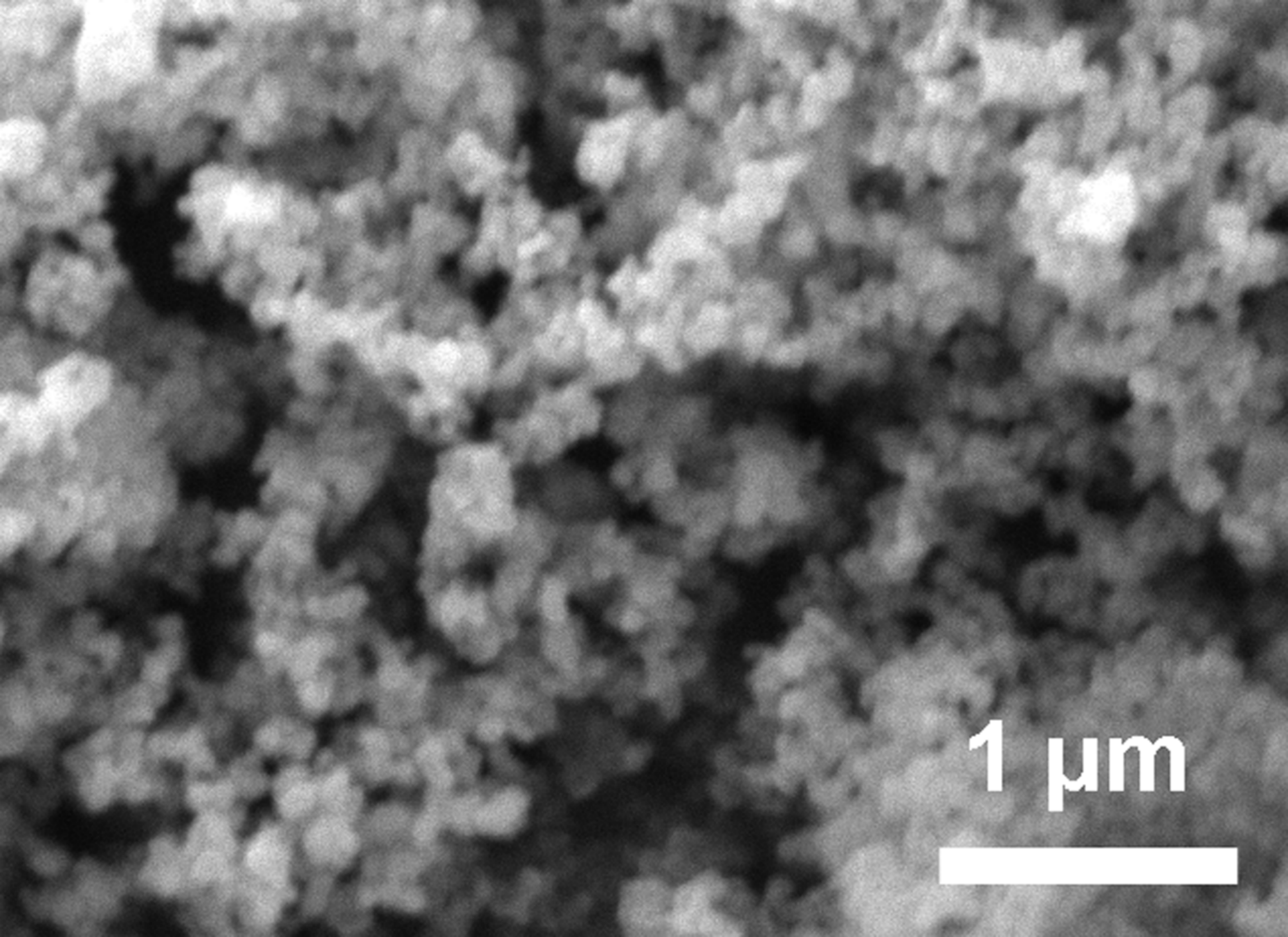
1 µm

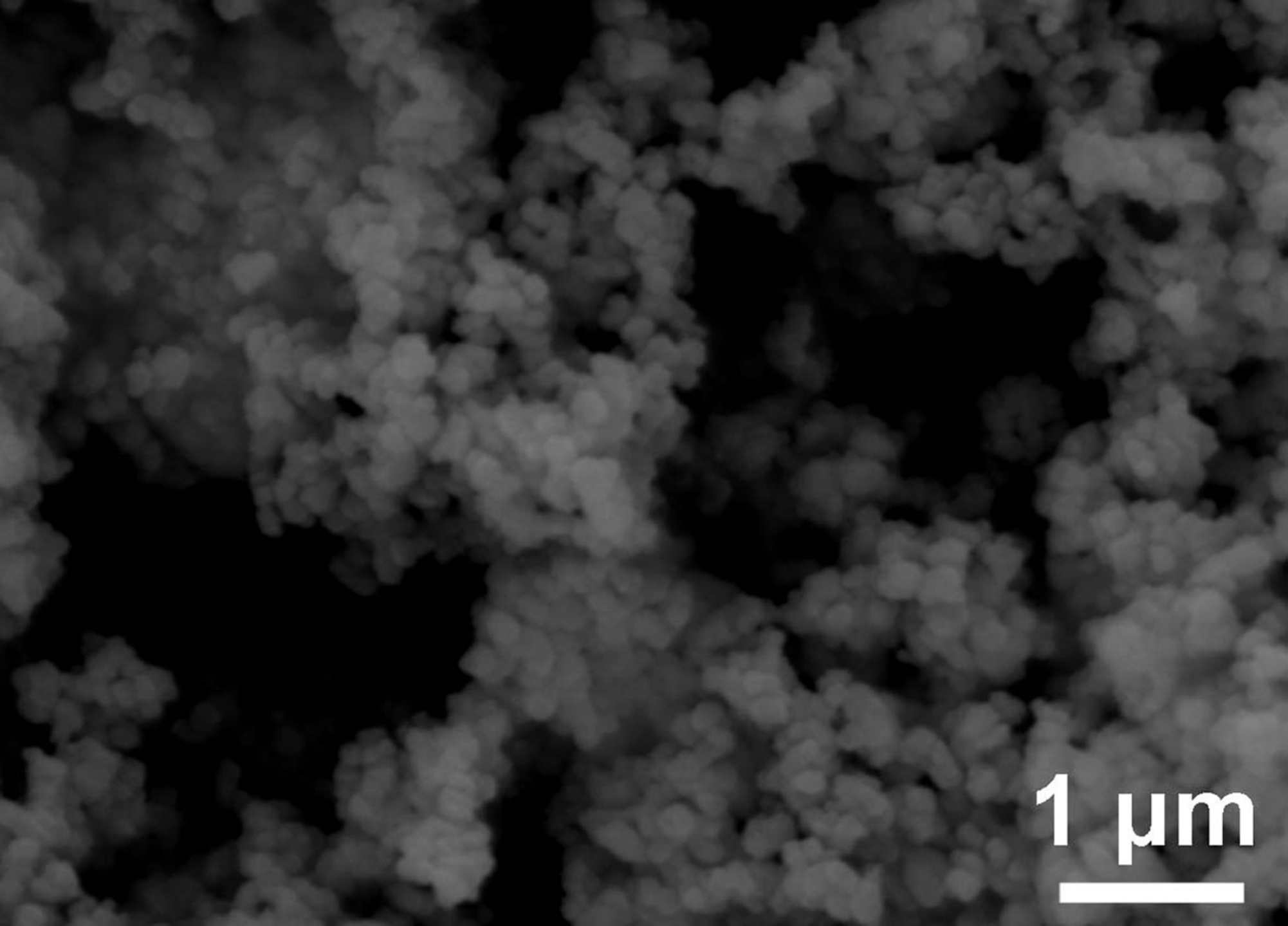
1 µm

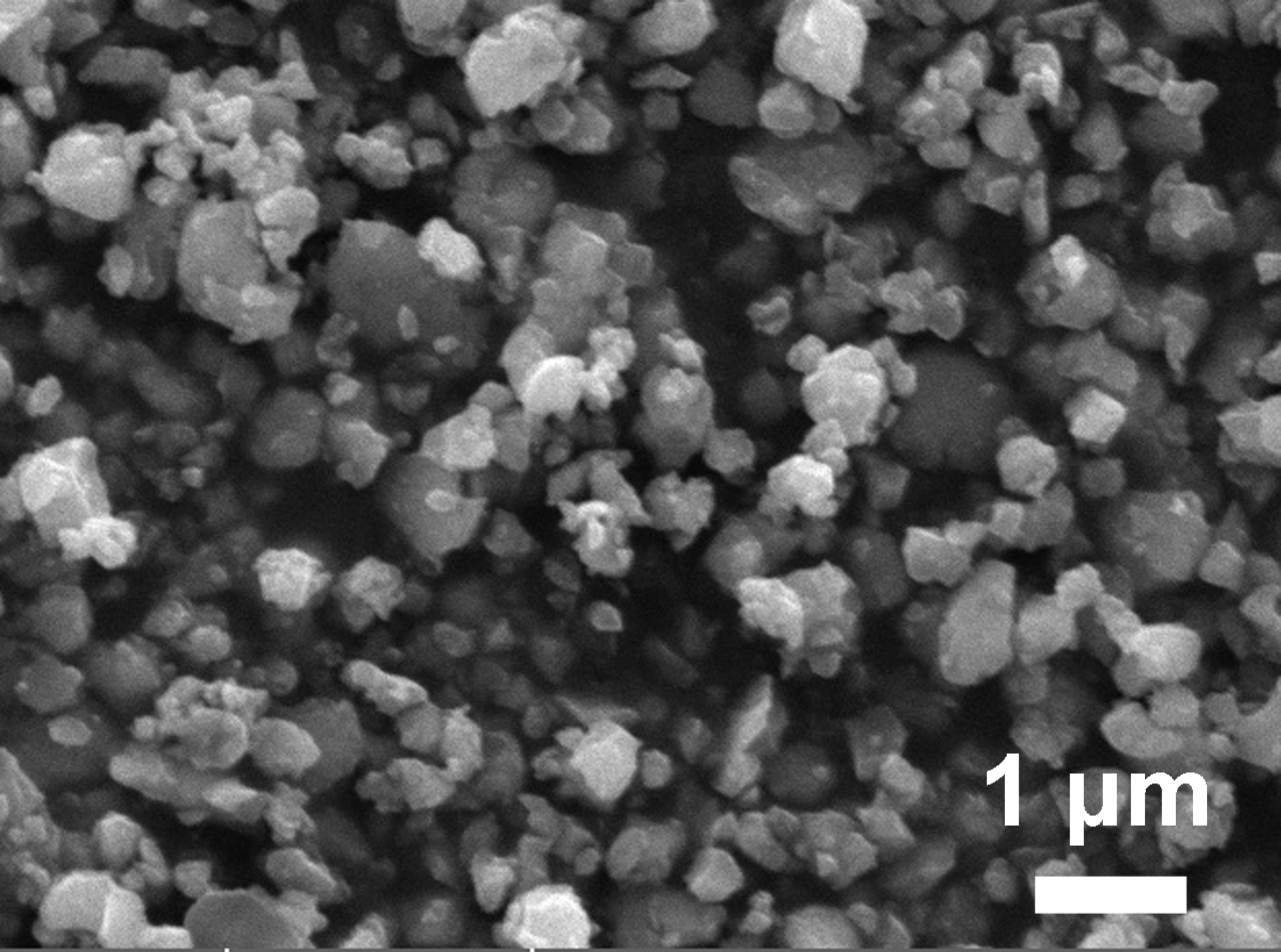
1 µm

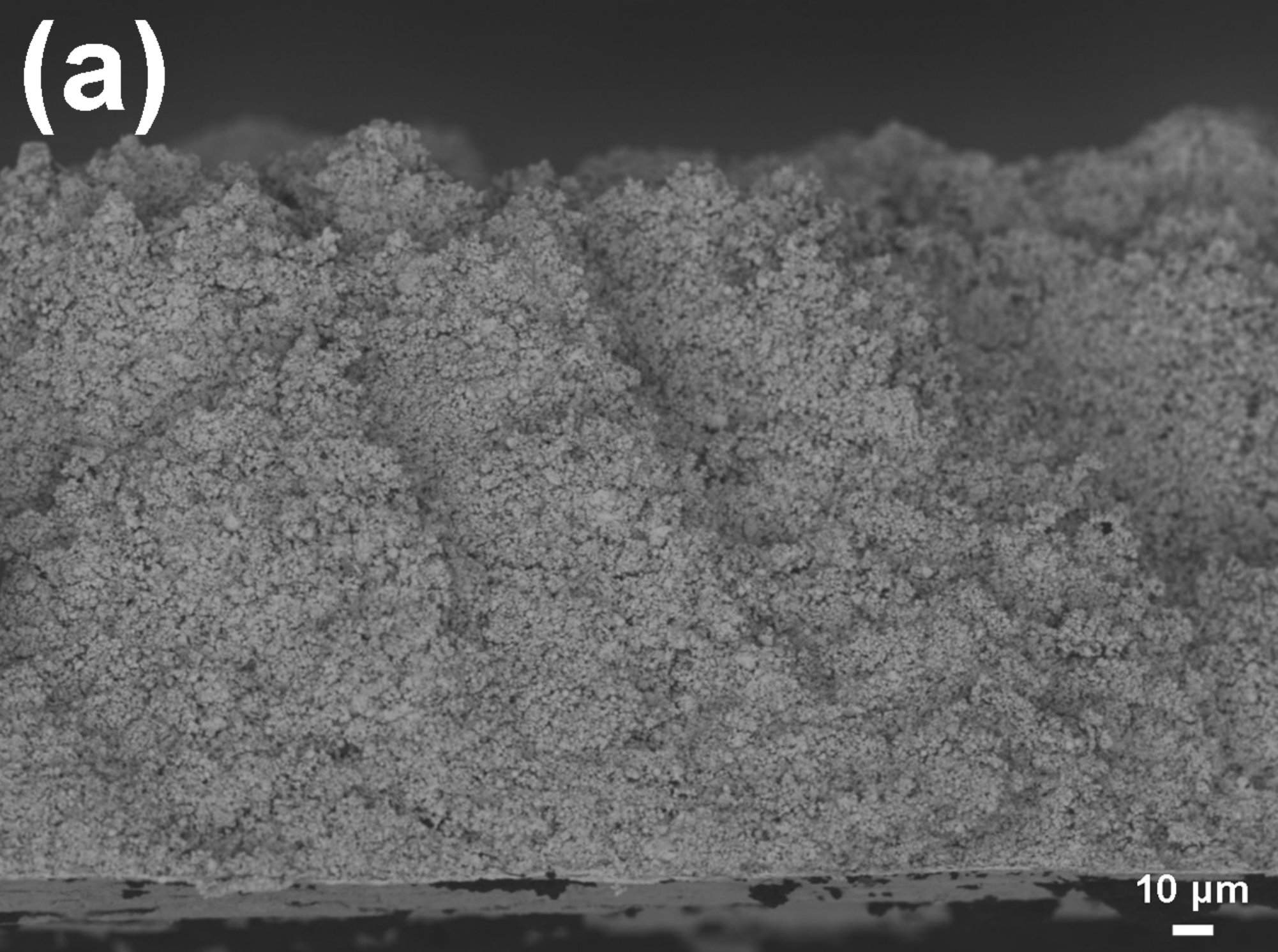
(a)
10 µm

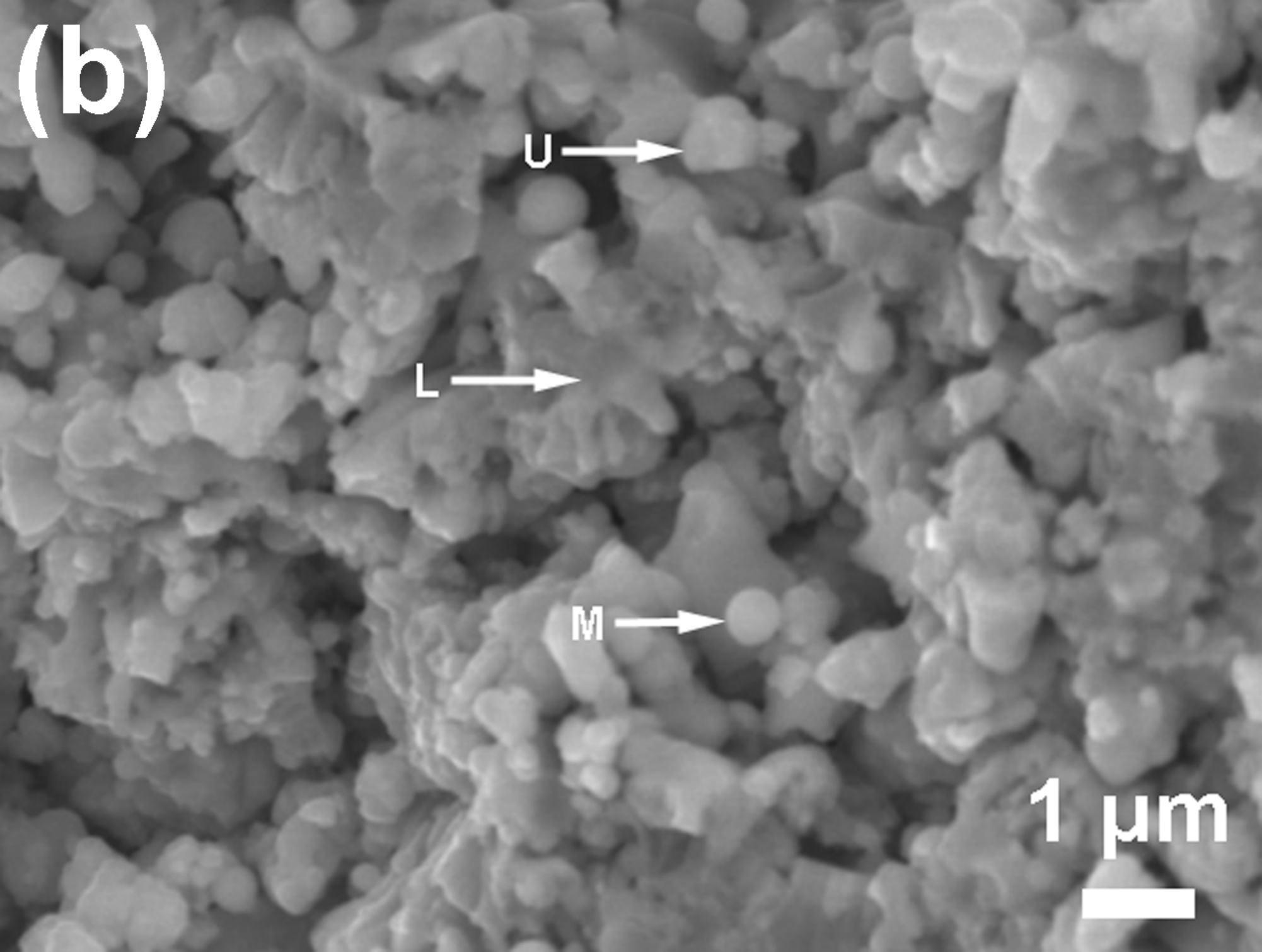
(b)
U
L
M
1 µm

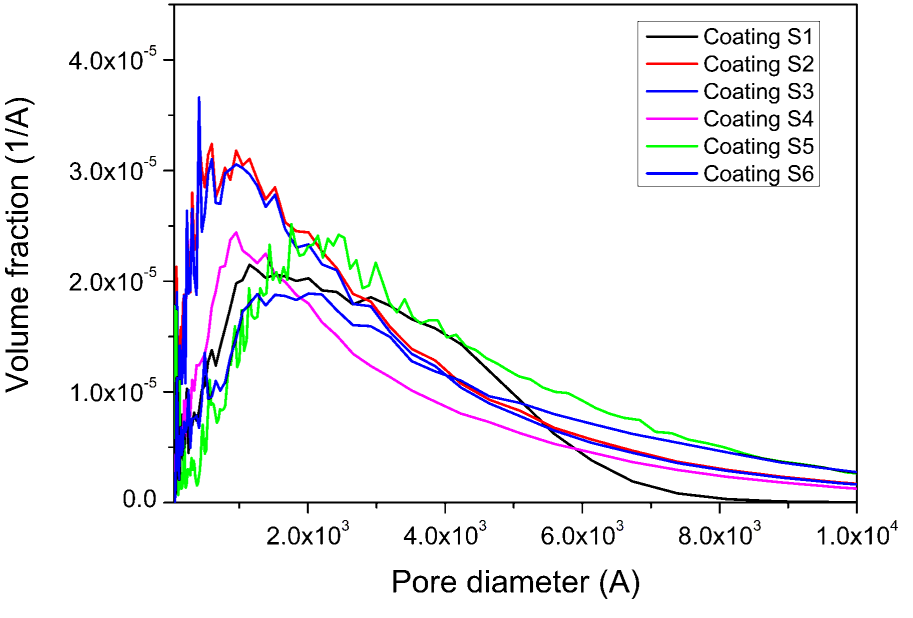
Coating S1
Coating S2
Coating S3
Coating S4
Coating S5
Coating S6
Volume fraction (1/A)
4.0x10-5
3.0x10-5
2.0x10-5
1.0x10-5
0.0
2.0x103
4.0x103
6.0x103
8.0x103
1.0x104
Pore diameter (A)

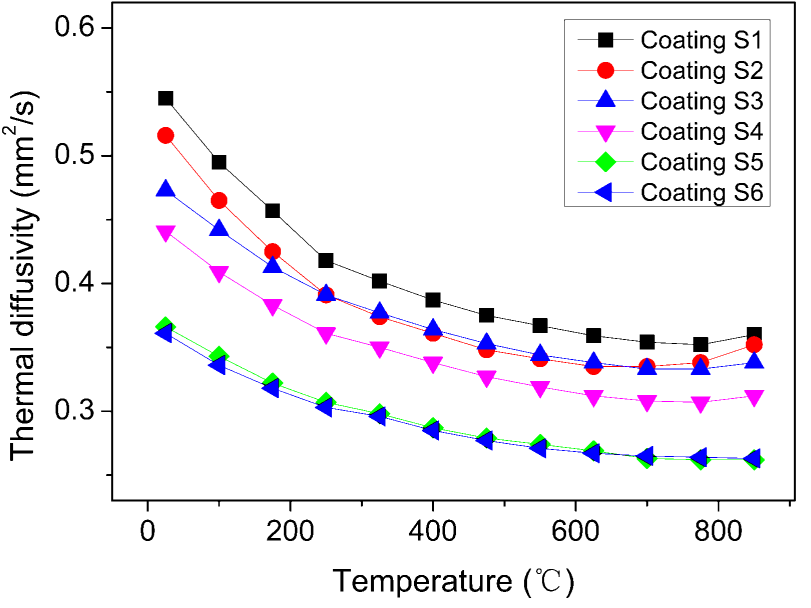
Thermal diffusivity (mm²/s)
0.6
0.5
0.4
0.3
0
200
400
600
800
Temperature (℃)
Coating S1
Coating S2
Coating S3
Coating S4
Coating S5
Coating S6

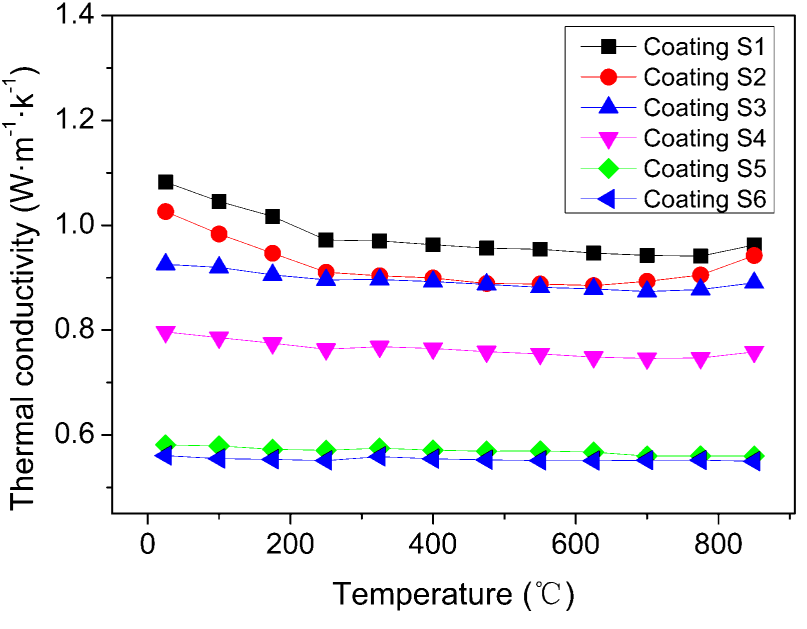
Thermal conductivity (W·m-1·k-1)
1.4
1.2
1.0
0.8
0.6
0
200
400
600
800
Temperature (℃)
Coating S1
Coating S2
Coating S3
Coating S4
Coating S5
Coating S6

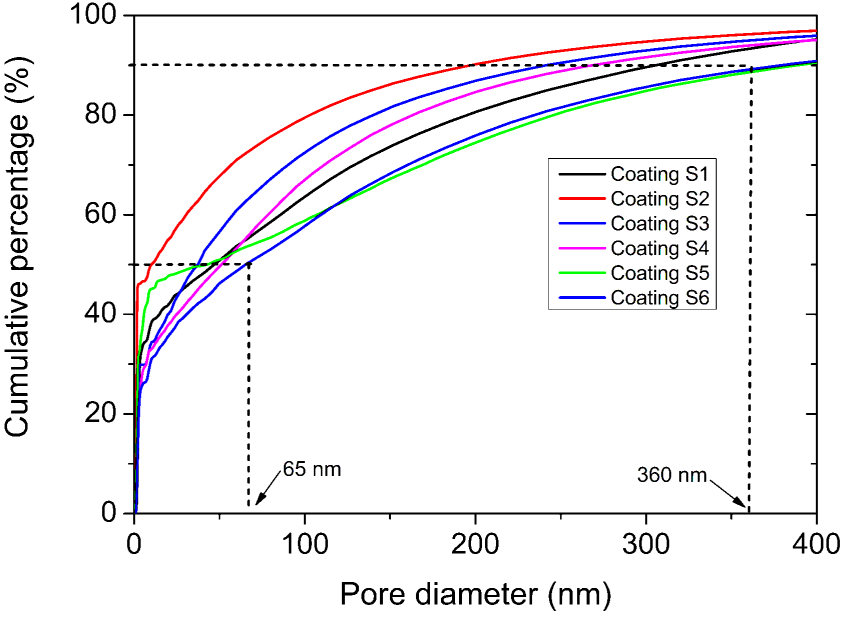
Cumulative percentage (%)
Pore diameter (nm)
0
20
40
60
80
100
0
100
200
300
400
Coating S1
Coating S2
Coating S3
Coating S4
Coating S5
Coating S6
65 nm
360 nm

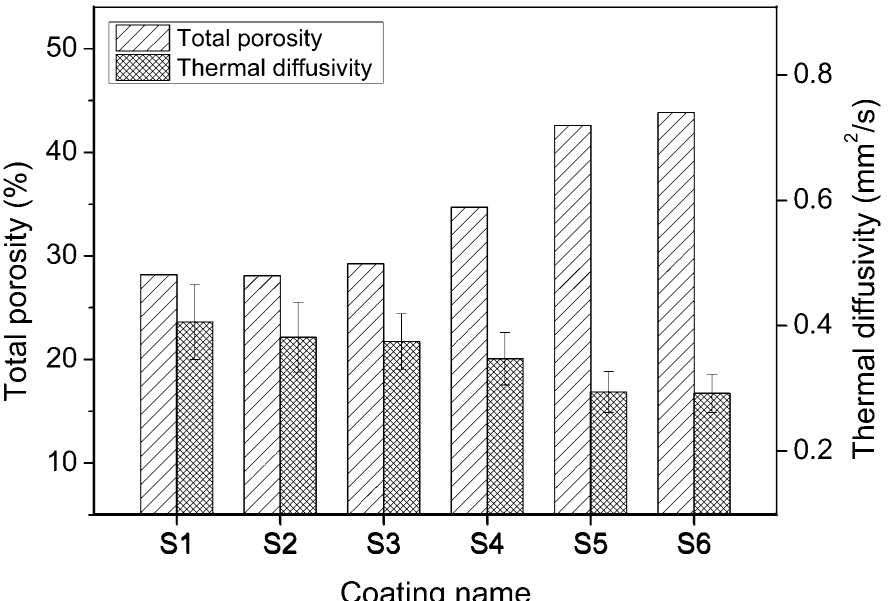
Total porosity
Thermal diffusivity
Total porosity (%)
Thermal diffusivity (mm²/s)
50
40
30
20
10
0.8
0.6
0.4
0.2
S1
S2
S3
S4
S5
S6
Coating name

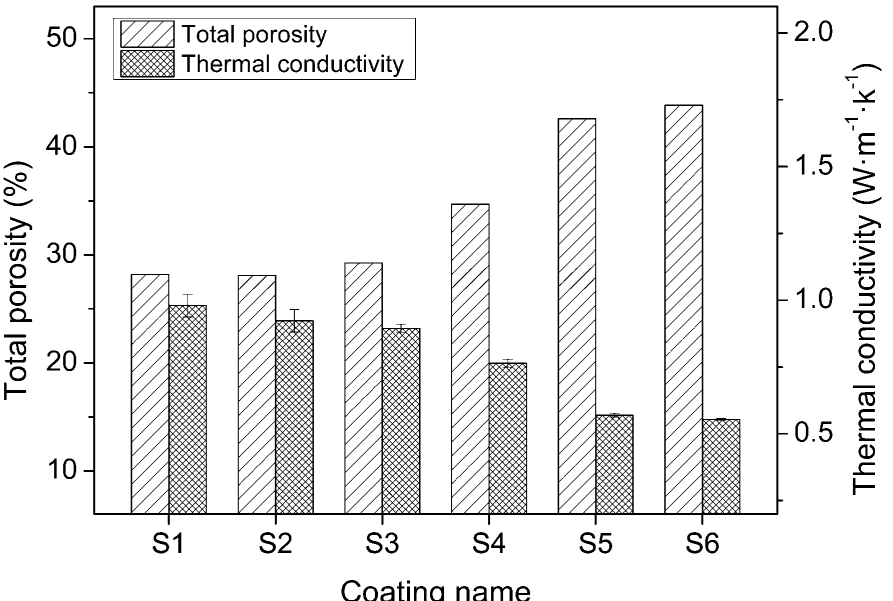
Total porosity
Thermal conductivity
Total porosity (%)
Thermal conductivity (W·m-1·k-1)
50
40
30
20
10
2.0
1.5
1.0
0.5
S1
S2
S3
S4
S5
S6
Coating name

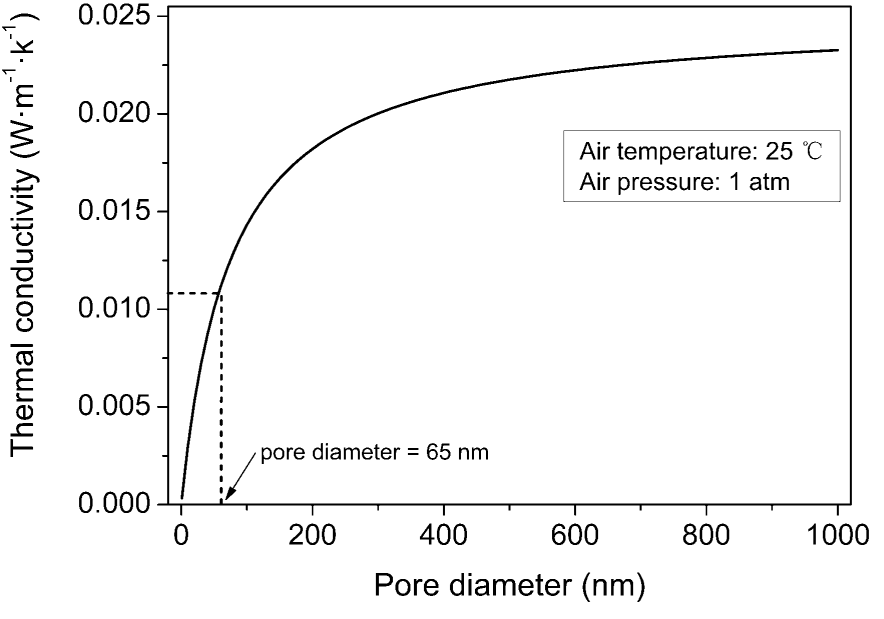
Thermal conductivity (W·m-1·k-1)
0.025
0.020
0.015
0.010
0.005
0.000
0
200
400
600
800
1000
Pore diameter (nm)
Air temperature: 25 ℃
Air pressure: 1 atm
pore diameter = 65 nm

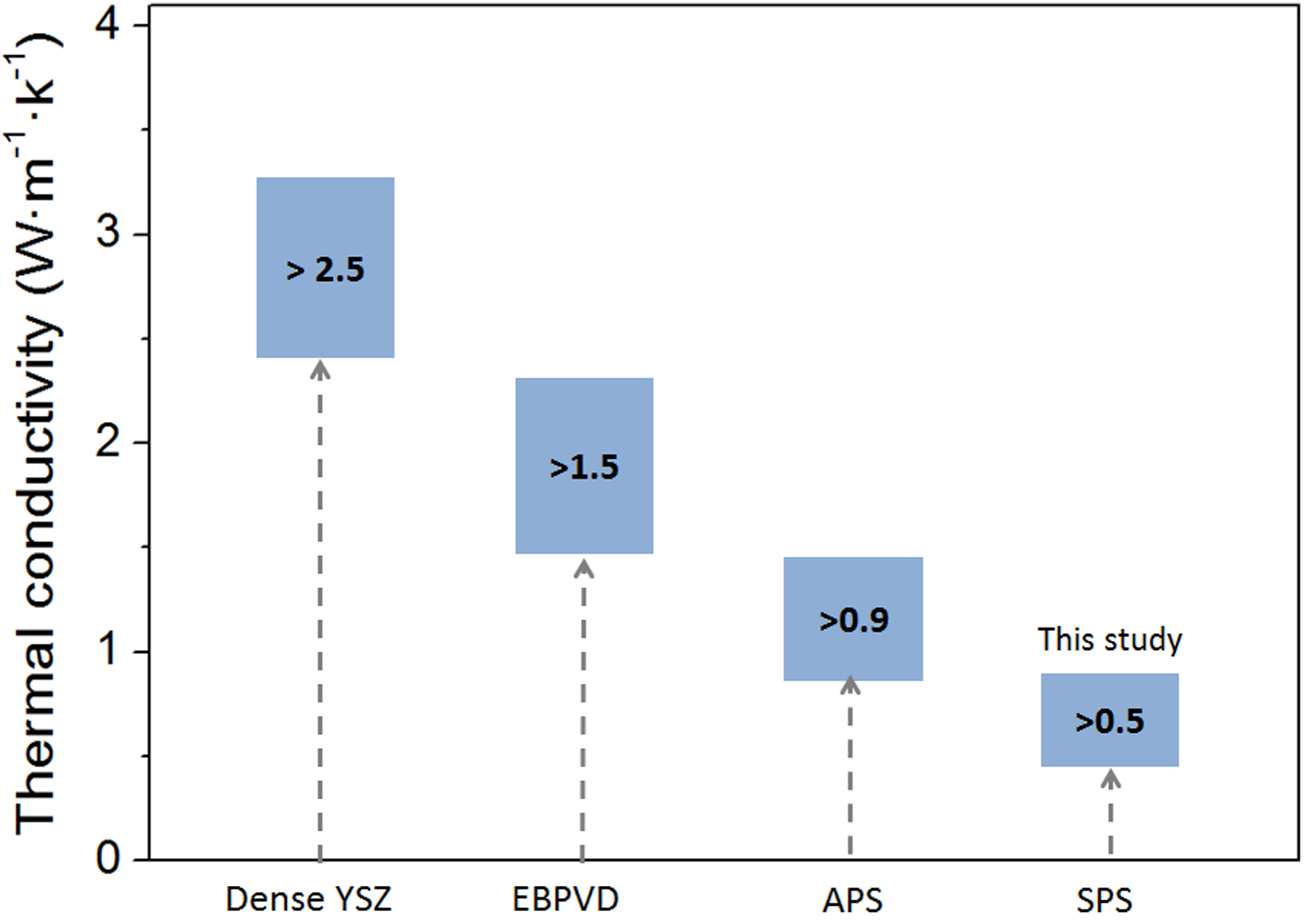
Thermal conductivity (W·m-1·k-1)
4
3
2
1
0
> 2.5
>1.5
>0.9
This study
>0.5
Dense YSZ
EBPVD
APS
SPS